Development of a carbon nanotube based microfocus x-ray tube with single focusing electrode

Zejian Liu[a)]
Department of Physics and Astronomy, University of North Carolina at Chapel Hill, Chapel Hill, North Carolina 27599

Jian Zhang
Department of Radiation Oncology, University of North Carolina at Chapel Hill, Chapel Hill, North Carolina 27599

Guang Yang
Department of Physics and Astronomy, University of North Carolina at Chapel Hill, Chapel Hill, North Carolina 27599

Yuan Cheng
Xintek Inc., P.O. Box 13788, 7020 Kit Creek Road, Research Triangle Park, North Carolina 27709

Otto Zhou and Jianping Lu
Department of Physics and Astronomy, University of North Carolina at Chapel Hill, Chapel Hill, North Carolina 27599 and Curriculum in Applied and Materials Sciences, University of North Carolina at Chapel Hill, Chapel Hill, North Carolina 27599

(Received 9 January 2006; accepted 27 March 2006; published online 10 May 2006)

We report a detailed study on the design of carbon nanotube based microfocus x-ray tube with one electrostatic focusing electrode. Based on the electron optics simulations, such parameters as geometrical distances and applied voltages among all the electrodes are considered, respectively, in relation to the size of x-ray focal spot. The stability of the x-ray focal spot size is also examined with respect to the variation of gate and anode voltages. Experimental results that agree well with the simulated data are also provided to corroborate the design method. We also discuss the operating stability and limitations when designing a carbon nanotube based microfocus x-ray tube with only one electrostatic focusing electrode. The designed x-ray tube with an isotropic focal spot sees wide applications in *in vivo* medical imaging studies. © *2006 American Institute of Physics.*
[DOI: 10.1063/1.2198793]

I. INTRODUCTION

X-ray microcomputed tomography (micro-CT) plays a key role in small animal imaging for disease studies and genetic manipulation.[1,2] A reliable correlation between the model structures and anatomy in small animal studies requires high spatial resolution, which depends primarily on the x-ray focal spot size, the pixel pitch of the detector, and the imaging geometry. By choosing the optimum geometry magnification and given the pixel pitch of current detector technology, the spatial resolution is really limited by the penumbral blurring of the x-ray focal spot.[3] Thus reducing the focal spot is essential in achieving high resolution for an x-ray micro-CT scanner. The x-ray focal spot is usually reduced by focusing the emitted electrons that impinge on the anode. Comparing to the electrostatic focusing,[4] magnetic lenses offer lower aberrations and better focusing properties.[5,6] However, the magnetic focusing unit is usually very awkward in size and requires complex power control unit. In contrast, electrostatic focusing only requires one or more simple metal electrodes and can be easily miniaturized.

Conventional x-ray tubes usually implement thermioinic cathode, where electrons are boiled out by heating the filaments to more than 1000 °C. This type of x-ray tube has been a reliable work horse for x-ray radiology with relatively low cost and high flux. However, they have several inherent limitations: (a) the tube cannot be easily miniaturized due to the high temperature cathode; (b) they have limited temporal resolution due to the slow response time of the thermionic emission; (c) high operating temperature reduces the lifetime of the x-ray tubes and increases the operating costs. These deficiencies limit the size, the speed, the flux, and the overall design flexibility of x-ray imaging systems.

Contrary to thermionic cathodes, carbon nanotube (CNT) based cathodes utilize field emission to generate electrons instead of high temperature heating. CNT usually has a small diameter of nanometer but a length of micrometer. This unique structure makes CNT excellent field electron emitters.[7–11] In addition, owing to the intrinsic instantaneous response time of the field emission process,[12] CNT based cathodes are able to offer improved temporal resolution. It has been demonstrated that CNT based x-ray source with a triode structure can generate diagnostic quality x-ray radiation with temporal resolution up to nanoseconds,[13–17] which is significantly better than that of the thermionic x-ray

[a)]Author to whom correspondence should be addressed; electronic mail: zejianl@physics.unc.edu

tubes.[18] By gating CNT based x-ray source with physiologically monitored signals, the motion-induced blurring during the process of imaging can be minimized, which is essential for the development of *in vivo* imaging systems.[19,20]

With the successful demonstration of ultrahigh temporal resolution, the achievement of high spatial resolution in the development of CNT based x-ray scanner depends critically on the focal spot size. In the prototype x-ray scanner developed in our group, a simple electrostatic electrode was inserted between the gating electrode and anode to harness the electron trajectories, thereby providing focused electron probe on the anode. An x-ray focal spot with a diameter of 250 μm has been illustrated for a cathode of 1 mm in diameter.[21] However, this system has yet been optimized with respect to further reducing the x-ray focal spot size. A systematic study of the parameters that affect the electron focusing in the CNT based x-ray tube is necessary for our further development of the x-ray imaging system.

Here we report a detailed study on the design of a CNT based microfocus x-ray tube with one focusing electrode. Based on a series of simulated data, several design criteria are proposed in achieving x-ray focal spot of various sizes. Experiment following a modeled x-ray tube design was implemented to verify the simulated results. We also discuss the operating stability and limitations of the thus-designed x-ray tube.

II. MODEL DESIGN AND SIMULATION

The model system of the microfocus x-ray tube studied here comprises a field emission cathode, a gate electrode, a focusing electrode, and an anode housed in a vacuum chamber as shown schematically in Fig. 1(a). The gating grid is modeled as equally spaced rings as shown in Fig. 1(b). The diameter of each ring is 40 μm, while the radial distance between two neighboring rings is 150 μm. Electrons are initially extracted from the CNT-deposited cathode by the strong electric field between the cathode and the gating grid (voltage set as V_g), and are then focused by the focusing voltage (V_f) before reaching the high-voltage (V_a) anode for the generation of x rays. A single focusing electrode, which is made of a metal plane diaphragm, was used in the current design of x-ray tube for electron focusing. The x-ray focal spot size is controlled by adjusting the various geometrical parameters as illustrated in Fig. 1(c) and the applied voltages on all electrodes.

The relation between x-ray focal spot size and the respective geometrical parameters is simulated in the commercial electron optics software (LORENTZE developed by Integrated Engineering Software Inc.). The electrostatic potential distribution and electric field among all electrodes are calculated based on the finite element analysis with about 3000 triangular meshes, while the electron trajectories are simulated according to Newton's equations. Electrons are field emitted from the CNT-deposited cathode due to the electric field between gate and cathode. After electrons transmit the gating grid with some divergence angle, their trajectories are controlled by the focusing electrode and anode. In the simulation, we ignore the field emission properties of electrons

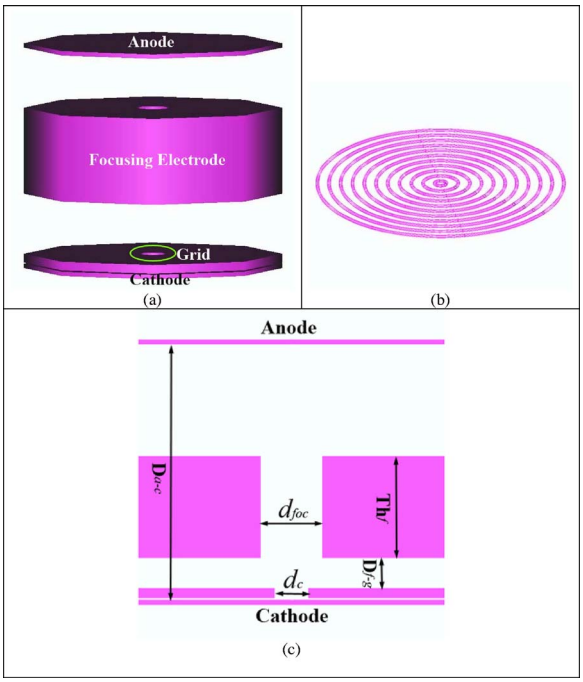

FIG. 1. (a) Schematic of a microfocus x-ray tube consisting of a cathode, a gate, a focusing electrode, and an anode. All the apertures in the electrodes are rotationally symmetrical with respect to the cathode-to-anode axis. (b) Enlarged view of the emission grid inside the circled area in (a). (c) Cross-sectional view of the x-ray tube in (a) where $D_{a\text{-}c}$ denotes the axial distance between the anode and cathode, D_{f-g} the axial distance between focusing and gate electrodes, d_c the diameter of cathode for field emission, d_{foc} the diameter of the focusing aperture, and Th_f the thickness of the focusing electrode.

from the carbon nanotube cathode and focus on the electron focusing behavior between gate and anode. Divergent electrons passing through the gating grid are evenly distributed with a radial spacing of 50 μm. A one-to-one correspondence between cathode diameter and electron distribution diameter above the gating grid is also assumed.

Figures 2(a)–2(e) shows the variation of the x-ray focal spot relative to the divergence angle of electrons emitted from the gating grid, where the cathode diameter is set at 1 mm and all the other parameters used in the simulation are listed in Table I. At the focusing voltage of 1000 V, the electron crossover position on the cathode-anode axis just impinges on the anode surface generating the x-ray focal spot of the minimum diameter. Figure 2(f) shows the variation of the focal diameter with respect to the divergence angle. When there is no divergence, i.e., all emitted electrons travel along the tube axis, the smallest x-ray focal diameter is achieved for a certain cathode size. Then the focal spot size increases monotonically with the divergence angle. Due to field emission, extracted electrons from cold cathode usually travel along the electric fields and thus a small divergence angle is usually observed. In all the following simulations, a divergence angle of ±4° will be readily assumed, which is in agreement with the experimental results as discussed later on.

For the same tube design, we also note that the x-ray focal spot size is proportional to the diameter of the field emission cathode, as illustrated in Fig. 2(g). For a cathode as

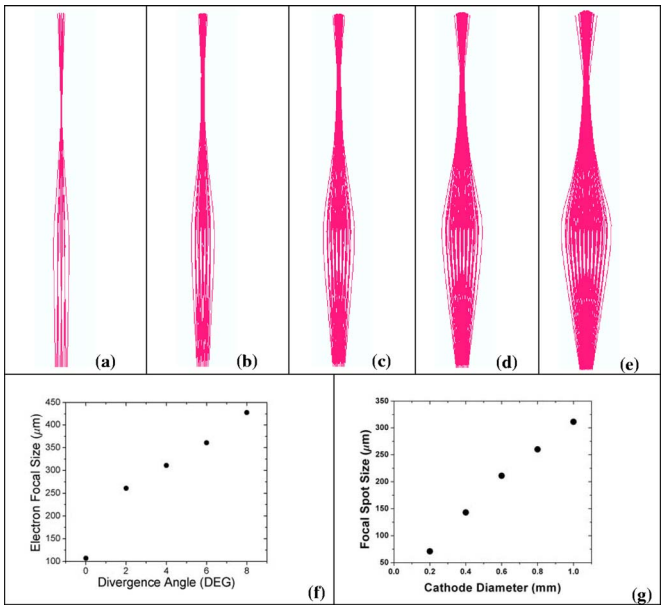

FIG. 2. For a set of given parameters for the x-ray tube as listed in Table I, the x-ray focal spot diameter d_f varies with the divergence angle of electrons passing through the gating grid (a)–(e), and the results are shown in (f). (g) Variation of the x-ray focal spot size relative to the diameter of the emissive cathode at the divergence angle of ±4°, which is in agreement with the experimental measurement.

small as 0.2 mm in diameter, the x-ray focal diameter d_f can be reduced down to 71 μm, while d_f increases up to 311 μm for a cathode diameter of 1 mm. Considering the takeoff angle of 6° in the x-ray tube projection geometry, a projected focal spot size of less than 10 μm can be easily achieved with a 0.2 mm diameter cathode as illustrated in Fig. 2(g). Therefore, given the potential of offering high current density in CNT based field emission cathode, decreasing the cathode dimension provides a viable way of reducing the x-ray focal spot size.

TABLE I. Parameters in the experimentally designed microfocus x-ray tube.

$D_{a\text{-}c}$ (cm)	D_{f-g} (cm)	Th_f (cm)	d_{foc} (cm)	D_c (cm)	V_g (V)	V_f (V)	V_a (kV)
2.5	0.3	1.0	0.6	0.1	1000	1000	40

The x-ray focal spot size is also very sensitive to the variation of the geometrical parameters that are illustrated in Fig. 1(c). In order to pursue an optimum geometry for designing microfocus x-ray tubes, we choose to separate them into individual factors in relation to the x-ray focal spot diameter. For comparison convenience, we assume that the diameter of the field emission cathode is 1 mm and that the emission divergence angle from the gating grid is ±4°.

Figure 3(a) shows the variation of the x-ray focal spot size with respect to the distance $D_{f\text{-}g}$ between the focusing electrode and gate. X-ray focal spot diameter decreases in a nonlinear way relative to the increase of $D_{f\text{-}g}$. However, the x-ray focal position on the cathode-anode axis is independent of $D_{f\text{-}g}$, and thus the focusing voltage keeps unchanged at 1500 V during the variation of $D_{f\text{-}g}$ as shown in Fig. 3(a). The focal diameter is reduced to 250 μm for a $D_{f\text{-}g}$ of 0.7 cm. The effect of increasing the thickness of focusing electrode Th_f on x-ray focal spot size is similar to that of increasing $D_{f\text{-}g}$ as shown in Fig. 3(b). The x-ray focal spot decreases against Th_f, although the axial focal position remains the same at 1500 V. The similarity between $D_{f\text{-}g}$ and Th_f originates from their same mechanism in electron focusing. By varying either $D_{f\text{-}g}$ or Th_f, the focal length of the

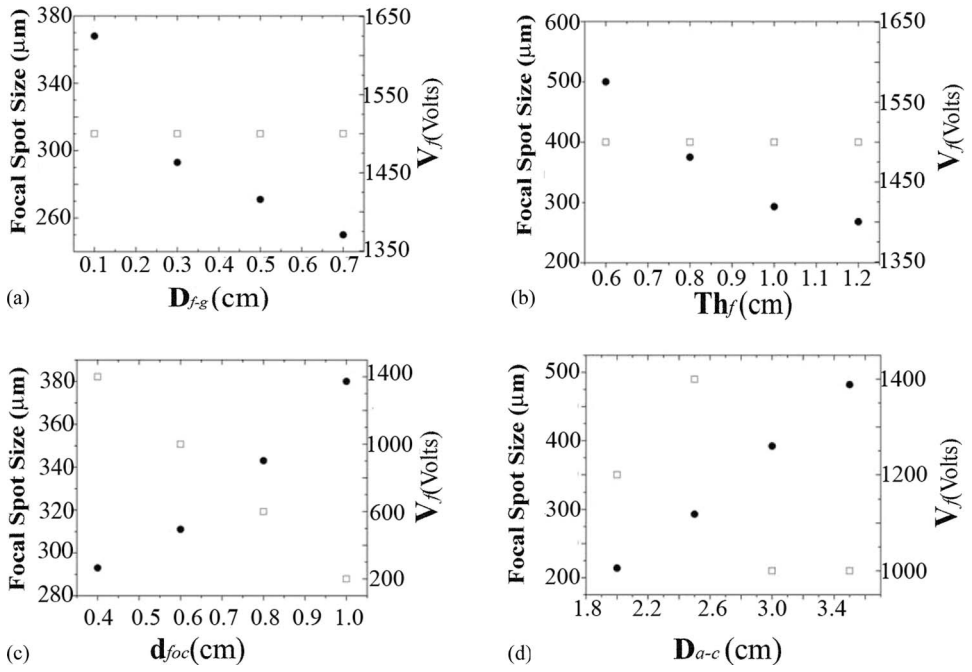

FIG. 3. Relationship (solid circles) between x-ray focal diameter and various geometrical parameters: (a) Distance between focusing electrode and gate D_{f-g}; (b) thickness of the focusing electrode Th_f; (c) diameter of the aperture of the focusing electrode d_{foc}; (d) distance between anode and cathode $D_{a\text{-}c}$. The variation of the optimum focusing voltage is also illustrated as the rectangles in (a)–(d), where the gate voltage V_g is kept at 1000 V. In (a)–(d), the default values for $D_{a\text{-}c}$, D_{f-g}, Th_f, and d_{foc} are set as 2.5, 0.3, 1.0, and 0.4 cm, respectively.

focusing electrode varies resulting in different magnifications that change the focal spot size. In this respect, reducing the distance between the upper surface of the focusing electrode and the anode offers stronger focusing, thereby resulting in smaller foci.

X-ray focal spot can also be reduced by decreasing the diameter d_{foc} of the focusing electrode aperture as illustrated in Fig. 3(c). By reducing d_{foc} from 1 to 0.4 cm, the x-ray focal spot is decreased by up to 30%. Further reducing d_{foc} would sacrifice a large amount of marginal electrons on the focusing electrode, although slight improvement in focal spot is still observed. Since varying d_{foc} changes the axial position of the electron crossover on the cathode-anode axis, the focusing voltage V_f needs be changed accordingly to keep the focal position on the anode surface. A linear relationship between V_f and d_{foc} can be deduced with a slope of about 2000 V/cm from Fig. 3(c).

Decreasing the distance ($D_{a\text{-}c}$) between the anode and cathode can also assist in reducing the size of x-ray focal spot as illustrated in Fig. 3(d), where the focal diameter decreases at the rate of 160 μm/cm relative to $D_{a\text{-}c}$ in the range between 2 and 4 cm. For example, the focal spot diameter is 211 μm with $D_{a\text{-}c}$ being 2 cm, while the focal diameter increases to 470 μm at a $D_{a\text{-}c}$ of 3.5 cm. Although the variation of the focusing voltage is necessary to keep the electron crossover on the anode surface, no direct relationship between V_f and $D_{a\text{-}c}$ is observed in Fig. 3(d).

III. EXPERIMENTAL RESULTS

A CNT based field emission x-ray tube has been constructed in experiment based on the simulated model system with the detailed parameters listed in Table I. The field emission CNT cathode was formed by depositing a uniform layer of randomly oriented small-diameter multiwalled carbon nanotubes (obtained from Xintek Inc.) on a metal substrate by electrophoretic deposition with fine control of the film thickness and morphology.[22] A commercially available tungsten grid with rectangular holes was used as the extraction gate electrode with the side length of each hole and the grid diameter being 180 and 40 μm, respectively. A slice of insulated mica spacer with a thickness of 150 μm was inserted between gate and cathode. The cathode-anode axis, mounted vertically in the vacuum chamber, was tilted by 6° relative to the source to detector direction in the x-ray imaging acquisition setup.

The emission properties of the field emission CNT cathode were characterized at the dynamical vacuum of 10^{-8} Torr. As shown in Fig. 4(a), electrons start to emit when the electric field is lower than 2 V/μm. The current-voltage relation follows the classic Fowler-Nordheim behavior as shown in the inset of Fig. 4(a). An emission current density of 10 mA/cm^2 was obtained at a threshold electrical field of ~2.6 V/μm. The emission stability and lifetime were also tested. After the initial aging process where arcing frequently occurs, the emission current becomes stable without electronic compensation at current levels required for small animal imaging. Figure 4(b) shows the variation of the emission current versus time measured under the dc mode (100% duty cycle) with the anode voltage and tube current set at 40 kV and 0.6 mA, respectively. With a ballast resistor, the emission current decays from 610 to 550 μA over a 40 h period with a local current fluctuation of 1%.

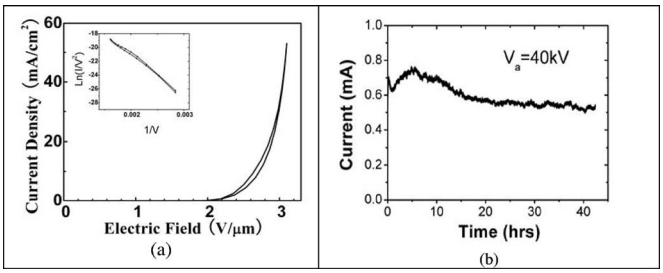

FIG. 4. (a) Field emission characteristic of a fabricated CNT based cathode of 2.5 mm in diameter. (b) Lifetime measurement of a CNT based cathode under the tube current and anode voltage of 0.6 mA and 40 kV, respectively.

The focal spot size of the CNT based x-ray tube was studied by measuring the edge spread function of a tungsten cross wire that has a diameter of 1.0 mm. In the imaging setup, the metal wire was mounted onto the center of the circular beryllium window where x rays exit. Then the projection angle of the x-ray focal spot at the center of the cross wire is about 14°. The x-ray intensity was recorded on the x-ray flat panel detector with the pixel pitch of 50 $\times$ 50 μm^2 (Hamamatsu Model C7921CA-02). Along the x-ray imaging axis, the distance between source and detector is 120 cm, while the distance between source and the metal wire is 12 cm. This gives a total imaging magnification of 10. To obtain enough x-ray flux for a significant signal-to-noise (SNR) ratio, the x-ray detector was operated at the 2 $\times$ 2 binning mode which results in the imaging pixel size of 100 $\times$ 100 μm^2. Thus the error of measuring x-ray focal diameter is $\pm$10 μm.

Given a circular focused electron probe of diameter d_f striking the anode surface, the projected x-ray focal spot becomes elliptical and is denoted as d_f (vertical) $\times d_f \tan(14°)$ (horizontal). Figure 5(a) shows an x-ray projection image of a tungsten cross wire. Following the European Standard EN 12543-5 in measuring the size of x-ray focal spot,[23] line intensity profile across the vertical wire in Fig. 5(c) gives a diameter of 320$\pm$10 μm for the x-ray focal spot size d_f, while the projected x-ray focal spot diameter is measured to be 80$\pm$10 μm from Fig. 5(b), which matches very well the simulated data for this x-ray tube design. To demonstrate the high spatial resolution of the CNT based microfocus x-ray tube, we imaged a resolution phantom. By setting the anode voltage at 40 kVp and using an exposure of 0.5 mA s, the source to object (STO) and source to detector distances (STD) were set at 20 and 32 cm, respectively, which results in a geometrical magnification of 1.6. Figure 5(d) shows an x-ray image of the resolution phantom where 10 lp/mm (lp denotes line pair) was clearly resolved as demonstrated in Fig. 5(e).

IV. STABILITY AND LIMITATIONS

Field emission from carbon nanotubes is usually operated at a constant current mode to keep the stability of the tube current. This requires that the gate voltage V_g changes

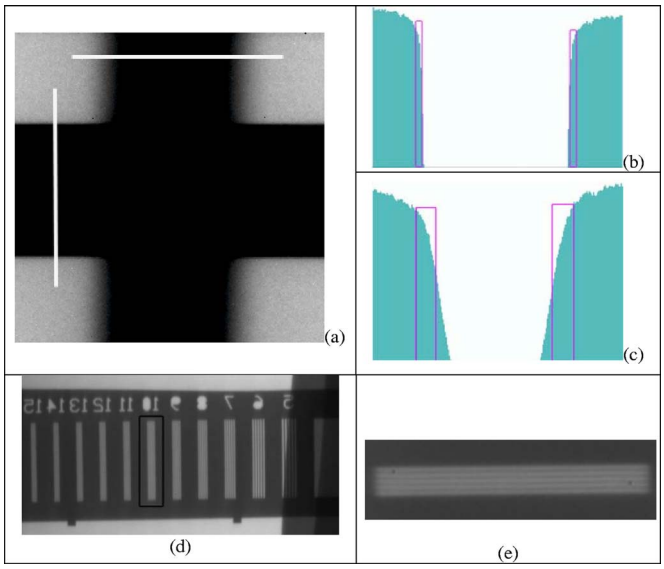

FIG. 5. (a) X-ray projection image of a tungsten cross wire (1 mm in diameter) acquired in our homemade x-ray scanner operated at 40 kVp and 25 mA s. Line intensity profiles across the horizontal and vertical branches of the cross are shown in (b) and (c), respectively. (d) Projection image of a test phantom which tells the resolution of the x-ray scanner. (e) Magnified view of the area in the black rectangle in (d), which illustrates the clearly resolved line pairs.

with time which may affect the focal spot size. Figure 6(a) shows the relationship between the focal spot size and the gate voltage given that the other parameters remain the same. Increasing the gate voltage enlarges the x-ray focal spot size linearly at a rate of 0.09 μm/V, while the electron crossover position on the anode-cathode axis keeps unchanged. Thus for a CNT based x-ray tube operated at a gate voltage of 800 V, a 20% variation of the gate voltage distorts the x-ray focal diameter by 1.4 μm, which is only about 1% the normal x-ray focal spot size.

The x-ray focal spot size is also dependent on the anode voltage as illustrated in Fig. 6(b). Higher anode voltage offers improved x-ray focal size. For example, the x-ray focal spot diameter decreases by up to 30% when we vary the anode voltage from 30 to 60 kV. The change of x-ray focal diameter is slower at high anode voltages than that at low anode voltages. But an average rate of 2.3 μm/kV is observed for the variation of focal diameter with respect to that of the anode voltage in the range of 30–60 kV. In addition,

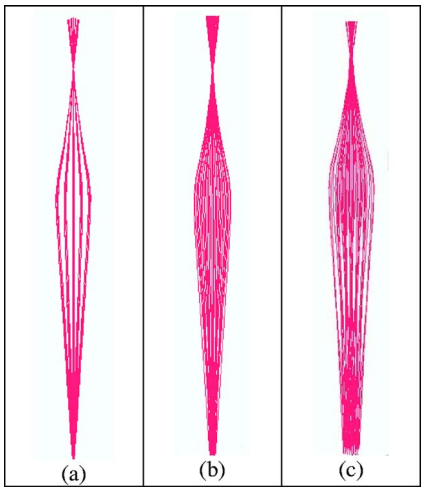

FIG. 7. Given the x-ray tube geometry: $D_{a\text{-}c}$=2.1 cm, D_{f-g}=1.4 cm, d_{foc} =0.4 cm, Th$_f$=0.1 cm, V_a=40 kV, V_g=1000 V, V_f=900 V, and the divergence angle of ±4° for electron emission from gate surface, the x-ray focal spot size is 35, 65, and 145 μm for the cathode diameter of (a) 0.1 cm, (b) 0.3 mm, and (c) 0.8 mm, respectively.

the axial focal position on the anode-cathode axis changes as a result of the variation of the anode voltage. To keep the axial focal position on the anode surface, we need to change the focusing voltage at a rate of 20 V/kV relative to the variation of the anode voltage as shown in Fig. 6(b).

Two practical limitations in x-ray tube design have to be considered for reducing the x-ray focal spot size by optimizing the geometrical parameters listed above: (a) small gap between the metal electrodes introduces arcing of x-ray tube thereby causing the failure of x-ray generation; (b) small apertures in thick focusing electrodes usually sacrifice a large amount of divergent electrons resulting in the inefficiency of x-ray production.

Based on the above suggestions, we vary the geometrical parameters such as $D_{a\text{-}c}$, $D_{f\text{-}g}$, Th$_f$, and d_{foc} simultaneously. Figure 7 shows the results with one set of good tube designs, where the x-ray focal diameter is 145 μm with the cathode diameter and emission divergence angle being 0.8 mm and ±4°, respectively. When the cathode size is narrowed down to 0.3 mm, the x-ray focal diameter becomes 65 μm as shown in Fig. 7(b). A focal diameter of 35 μm can be achieved by further reducing the cathode size to 0.1 mm as shown in Fig. 7(a). The smallest x-ray focal spot size that

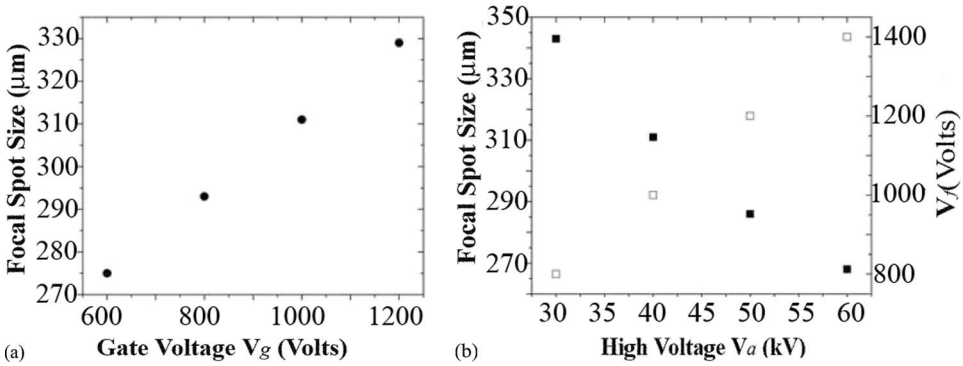

FIG. 6. Stability of the x-ray focal spot size with respect to the gate voltate V_g in (a) and the anode voltage V_a in (b), respectively. In (a) the focusing voltage kept at 1000 V, while in (b) the focusing voltage varies linearly with V_a. The geometrical parameters $D_{a\text{-}c}$, D_{f-g}, Th$_f$, and d_{foc} are set as 2.5, 0.3, 1.0, and 0.6 cm, respectively.

can be achieved for the tube design is theoretically limited by the spherical aberration of the electrostatic lens systems.[24] Due to spherical aberration, an ideal point electron source usually becomes a diffused crossover whose diameter is $0.5C_s\alpha^3$, where C_s is the spherical aberration coefficient, and α is the semidivergence angle of electron beams. For this specific tube design, the spherical aberration coefficient is calculated to be 10.5 cm. This means that, given a point electron source with a divergence angle of ±4°, the smallest electron crossover after focusing would have a diameter of 18 μm. This theoretical limitation cannot be overcome without a better design of electrostatic focusing electrodes.[25]

One important application of the microfocus x-ray source is cone-beam micro-CT imaging,[26] which desires a small isotropic x-ray source for obtaining isotropic voxels in volume image reconstruction. The capability of achieving smaller focal diameter by reducing the size of cathode offers us the capability of producing an isotropic x-ray focal spot given the desired focusing geometry. By designing an elliptical cathode with a dimension of 0.8×0.1 mm^2, a focal spot with the dimension of 145×35 μm^2 can be achieved. By tilting the anode-cathode axis by 14° along the longer dimension (i.e., 145 μm), we obtain an isotropic x-ray focal spot of 35×35 μm^2. Due to the observation that the maximum power for a stationary-anode microfocus x-ray source approximately follows the empirical relationship:[27]

$$P_{\max} \approx 1.4(d_{f,\mathrm{FWHM}})^{0.88}, \text{ for } V_a \leqslant 40\mathrm{kV} \quad (1)$$

where $P_{\max}$ is the maximum x-ray tube power in watts and $d_{f,\mathrm{FWHM}}$ is the focal spot size in microns, we find that the isotropic x-ray source with a size of 35×35 μm^2 can deliver a continuous tube current up to 1.5 mA at 40 kVp. However, when the designed x-ray tube runs in the pulse mode, i.e., the electron beam is switched on only during the x-ray exposure which is a very small fraction of the total operation time, much higher tube current than 1.5 mA can be achieved due to more efficient thermal management. Given the potential current density of 10 A/cm^2 for CNT field emission, a cathode current up to 8 mA can be obtained with an effective focal spot of 35 μm in diameter. Considering the limitation of signal to noise ratio in micro-CT imaging, we are able to generate x-ray pulses with a pulse width less than 10 ms. This allows us to turn on a single pulse for x-ray exposure only within a small portion of the physiological period of small animals and thereby reduce significantly the motion-induced artifacts. Combining the fast gating capability and high spatial resolution, the CNT based microfocus x-ray tube sees wide applications in *in vivo* four-dimensional (4D) imaging of small animals in medical studies.[28–30]

V. DISCUSSIONS

X-ray focal spot affects tremendously the spatial resolution of a microfocus x-ray imaging scanner. By introducing one focusing electrode in CNT based x-ray tube, it is possible to confine electron trajectories in a desired shape and thereby form suitable electron crossover on the anode surface for generating small x-ray focal spot. We found that a well-designed microfocus field emission x-ray tube should possess the geometrical features of (a) a small distance between the anode and the focusing electrode, and (b) reduced focusing aperture size. Such type of x-ray tube may be used to generate x-ray focal spot of different sizes in control by varying the emission area on the cathode and the emissive divergence angle at the gating grid. Experimental data that match very well with the simulated data are provided in the design of CNT based microfocus x-ray tube. This type of microfocus x-ray tube can deliver stable focal spot size with high enough flux and operate for an extended period of time.

ACKNOWLEDGMENTS

The carbon nanotube samples for making CNT based cathode was provided by Dr. B. Gao from Xintek Inc. We also thank Dr. Y. Z. Lee and Q. Qiu for their suggestive discussions in preparing the manuscript. This work was partially supported by the grants from NIH-NIBIB (Grant No. 1R21EB004204-01), the Transportation Security Administration (Manhattan II Project), and Xintek Inc.

[1] M. J. Paulus, S. S. Gleason, S. J. Kennel, P. R. Hunsicker, and D. K. Johnson, Neoplasia **2**, 62 (2000).
[2] E. L. Ritman, J. Cell. Biochem. **87**, 116 (2002).
[3] J. Selman, *The Fundamentals of Imaging Physics and Radiobiology*, 9th ed. (Springfield, IL, 2000).
[4] W. Ehrenberg and W. E. Spear, Proc. Phys. Soc. London, Sect. B **64**, 67 (1951).
[5] A. E. de Barr and I. MacArthur, Br. J. Appl. Phys. **1**, 305 (1950).
[6] U. W. Arndt, J. V. P. Long, and P. Cuncumb, J. Appl. Crystallogr. **31**, 936 (1998).
[7] M. S. Dresselhaus, G. Dresselhaus, and P. Avouris, *Topics in Applied Physics* (Springer-Verlag, Heidelberg, 2000), Vol. 80.
[8] W. A. de Heer, A. Chatelain, and D. Ugarte, Science **270**, 1179 (1995).
[9] A. G. Rinzler *et al.*, Science **269**, 1550 (1995).
[10] O. Zhou, H. Shimoda, B. Gao, S. J. Oh, L. Fleming, and G. Z. Yue, Acc. Chem. Res. **35**, 1045 (2002).
[11] W. Zhu, C. Bower, O. Zhou, G. Kochanski, and S. Jin, Appl. Phys. Lett. **75**, 873 (1999).
[12] R. Gomer, *Field Emission and Field Ionization* (Harvard University Press, Cambridge, MA, 1961).
[13] O. Zhou and J. P. Lu, U.S. Patent No. 6,553,096 (22 April 2003).
[14] O. Zhou and J. P. Lu, U.S. Patent No. 6,850,595 (1 February 2005).
[15] H. Sugie, M. Tanemura, V. Filip, K. Iwata, K. Takahashi, and F. Okuyama, Appl. Phys. Lett. **78**, 2578 (2001).
[16] G. Z. Yue *et al.*, Appl. Phys. Lett. **81**, 355 (2002).
[17] Y. Cheng, J. Zhang, Y. Z. Lee, B. Gao, S. Dike, W. Lin, J. P. Lu, and O. Zhou, Rev. Sci. Instrum. **75**, 3264 (2004).
[18] E. Sato *et al.*, Med. Biol. Eng. Comput. **32**, 295 (1994).
[19] C. J. Ritchie, J. Hseih, M. F. Gard, J. D. Godwin, Y. Kim, and C. R. Crawford, Radiology **190**, 847 (1994).
[20] J. C. Hu, S. T. Haworth, R. C. Molthen, and C. A. Dawson, Acad. Radiol. **11**, 961 (2004).
[21] J. Zhang *et al.*, Rev. Sci. Instrum. **76**, 094301 (2005).
[22] B. Gao, G. Z. Yue, Q. Qiu, Y. Cheng, H. Shimoda, L. Fleming, and O. Zhou, Adv. Mater. (Weinheim, Ger.) **12**, 1770 (2001).
[23] European Committee for Standardization, EN 12543-5: E. Brussels (1999).
[24] A. V. Crewe, J. Wall, and L. M. Welter, Rev. Sci. Instrum. **39**, 576 (1968).
[25] G. H. N. Riddle, J. Vac. Sci. Technol. **15**, 857 (1978).
[26] M. J. Paulus, S. S. Gleason, M. E. Easterly, and C. J. Foltz, Lab Anim. **30**, 36 (2001).
[27] M. J. Flynn, S. M. Hames, D. A. Reimann, and S. J. Wilderman, Nucl. Instrum. Methods Phys. Res. A **353**, 312 (1994).
[28] C. T. Badea, L. W. Hedlund, and G. A. Johnson, Med. Phys. **31**, 3324 (2004).
[29] C. T. Badea, B. Fubara, L. W. Hedlund, and G. A. Johnson, Mol. Imaging **4**, 110 (2005).
[30] D. Cavanaugh, E. Johnson, R. E. Price, J. Kurie, E. L. Travis, and D. D. Cody, Mol. Imaging **3**, 55 (2004).